



Contents lists available at ScienceDirect

Physics Letters A

[www.elsevier.com/locate/pla](http://www.elsevier.com/locate/pla)

# The Sun is the climate pacemaker I. Equatorial Pacific Ocean temperatures

David H. Douglass\*, Robert S. Knox

Department of Physics and Astronomy, University of Rochester, Rochester, NY 14627-0171, United States

## ARTICLE INFO

### Article history:

Received 27 August 2014  
Received in revised form 9 October 2014  
Accepted 10 October 2014  
Available online xxxx  
Communicated by V.M. Agranovich

### Keywords:

Climate  
Climatology  
Solar forcing  
Seasonal effects  
Phase locking  
El Niño

## ABSTRACT

Equatorial Pacific Ocean temperature time series data contain segments showing both a phase-locked annual signal and a phase-locked signal of period two years or three years, both locked to the annual solar cycle. Three such segments are observed between 1990 and 2014. It is asserted that these are caused by a solar forcing at a frequency of 1.0 cycle/yr. These periodic features are also found in global climate data (following paper). The analysis makes use of a twelve-month filter that cleanly separates seasonal effects from data. This is found to be significant for understanding the El Niño/La Niña phenomenon.

© 2014 Elsevier B.V. All rights reserved.

## 1. Introduction

In a detailed study of the equatorial Pacific sea surface temperature (SST) index  $SST_{3.4}$ , Douglass [1] found two signals, one that was predominantly 1.0 cycle/yr, and one of low frequency ( $<1.0$  cycle/yr) exhibiting the familiar El Niño/La Niña phenomenon. These were called  $N_H$  and  $N_L$ , respectively.  $N_L$  was found to contain time segments showing periodicities of multiples of one year. Ten such numbered segments were identified in the period 1870–2008 (see Table 3 of Ref. [1]). Either the beginning or end date, or both, of those segments had a near one-to-one correspondence with previously reported abrupt climate changes or climate shifts (CS). The two most recent of these segments studied were: 1991–1999, showing periodicity of three years, and 2001–2008, showing periodicity of two years. These, and the 1 cycle/yr component, were phase locked to the annual solar cycle. “Phase-locked” in what follows always refers to the solar cycle as reference. By phase locking we mean that a signal of frequency  $f_1$  has a fixed phase with respect to that of a second signal of frequency  $f_2 = (n/m)f_1$ , where  $n$  and  $m$  are integers. The relationship is usually a result of a non-linear mechanism. For application to geophysical time series, see [1,2] and Section 5.

To explain the various phenomena it was concluded that this climate system is driven by a forcing  $F_S$  of solar origin at a fre-

quency of 1.0 cycle/yr that causes the principal component of the direct response  $N_H$ . In addition,  $F_S$  may have caused the subharmonic response in  $N_L$  via some nonlinear mechanism.

Four additional atmospheric and surface climate indices exhibit the same periodic behavior [3] in the same segments: atmospheric pressure variation in the western Pacific; temperature anomalies in the tropical troposphere;  $PDO$ , a dimensionless index based upon temperature measurements north of  $20^\circ N$ ; and tropical wind.

It is of course not surprising that an annual signal is found in all the ocean–atmospheric climate indices. This, along with qualitative recognition of the superimposed subharmonics signaled by the El Niño/La Niña phenomenon, has been recognized for over 100 years. A chronology of observations of phase locking was presented in Ref. [1]. The present study revisits the Pacific sea surface temperature index  $SST_{3.4}$  starting from 1990, extends it through 2013, and presents a formal critique of the “climatology” method of removing seasonal (annual) components from data.

Section 2 describes the data sets, methods, and background material. The results are analyzed and discussed in Section 3. Section 4 considers related issues and Section 5 contains a summary of the conclusions.

## 2. Data and methods

### 2.1. Data

This study considers only data from the period January 1990 through December 2013.

\* Corresponding author.

E-mail address: [douglass@pas.rochester.edu](mailto:douglass@pas.rochester.edu) (D.H. Douglass).

*SST3.4*: Region 3.4 of SST is the equatorial Pacific (latitude 5°S to 5°N and longitude 120°W to 170°W), which is commonly used to study the El Niño Southern Oscillation (ENSO) phenomenon. The geographical average SST of Region 3.4 is named *SST3.4* and ranges between 24 °C and 30 °C. A widely used anomaly index is *Nino3.4*, which is *SST3.4* with the seasonal effect supposedly removed. The Climate Prediction Center of NOAA posts monthly values of both *SST3.4* and *Nino3.4* that begin in 1982 [4].

2.2. *Methods: precise separation of high- and low-frequency effects*

Studies of many geophysical phenomena start with a parent signal  $G_0$ , such as a temperature or wind speed record, containing a component of interest mixed in with a seasonal component at frequencies of 1.0 cycle/yr and its harmonics. The component of interest might show ENSO effects with multi-year periodicity. An important task is to separate the seasonal component from  $G_0$  to obtain the one of interest. A moving average is one of the methods used to make this separation. Such a filter of length one year, which we denote by an operator  $F$ , is the most precise for seasonal components, as Douglass [5] has shown in a study of *SST3.4* (the parent signal). He showed in some detail that the remaining seasonal signal should be considered an essential component of the ENSO phenomena and be retained for study.

In the present analysis only anomalies are treated. Thus we replace a parent series  $G_0$  by  $G = G_0 - \langle G_0 \rangle$ , where  $\langle G_0 \rangle$  is the average of the parent series over the period January 1990 to December 2013.

The filter  $F$  is applied to the series  $G$  to create a “season-free” anomaly  $aG$  defined as

$$aG = F(G). \tag{1}$$

This low frequency signal may contain the familiar ENSO phenomena. A “high frequency” index is also defined,

$$hG = G - F(G), \tag{2}$$

which contains a coherent signal at 1.0 cycles/yr and its harmonics, along with noise.

2.3. *Comparison with the climatology method*

The low frequency index given by Eq. (1) poses a direct challenge to the commonly used climatology method of removing the seasonal effect. The climatology method for the case of monthly data consists of (1) creating a climatology function  $C$  which, for any given month, consists of the average over the values for each such month in the range of  $G$ ; by definition the resulting time series  $C(G)$  has periodicity one year, and (2) defining the low-frequency residual index  $aG_C$  as

$$aG = G - C(G). \tag{3}$$

Mathematically, the series  $C(G)$  consists of a periodic function of period 1.0 year with zero mean plus a constant that is the average of  $G$ . In the case of *SST3.4* the climatology scheme fails to remove all of the seasonal effect, as we show below. The  $F$ -filter method does remove it [5] because, in addition to its obvious similarity to a low pass filter that allows frequencies lower than 1.0 cycle/yr to pass with only slight attenuation, it has another property that is not generally recognized. The Fourier transform of  $F(G)$  contains a factor  $H_{12}(f) = \sin(12\pi f) / \sin(\pi f)$ , which has zeros at multiples of the frequency  $f = (1/12) \text{ month}^{-1}$  [6]. Thus, components of  $F(G)$  whose frequencies are exactly  $f = (1/12) \text{ month}^{-1}$  and its harmonics are completely removed. This second property is highly desirable in reducing the seasonal signal that contains an annual component and its harmonics. One frequently sees the use

of  $k$ -month filters where  $k$  has values 3, 5, 7, 9, 11, 12, 13 in attempts to reduce the seasonal signal; the  $k = 12$  filter is obviously best for removal of such a signal. The data considered in this paper are either monthly (12 values/yr) or quarterly (4 values/yr). For the case of quarterly data the appropriate digital filter is a moving 4-point average.

Applying  $F$  to both sides of Eq. (3), one obtains

$$F(aG_C) = F[G - F(G)]. \tag{4}$$

Since  $F$  eliminates  $C(G)$  because of its pure periodicity, Eq. (4) becomes

$$F(aG_C) = aG. \tag{5}$$

This relation “repairs the damage” done by the climatology method and therefore proves useful when one has only an index generated by that method and no parent data.

In Appendix A an example of the filtering procedures is given, including a comparison of the 12-month filter and climatology methods. Application to El Niño data will be given in Section 4.

2.4. *Identifying phase-locked time segments*

Consider geophysical indices  $aG$  in which annual effects have been removed, and in which there exist time segments with components having periods that are exactly multiples of one year. One way of identifying these segments is to examine the autocorrelation function versus delay time  $\tau$  of a candidate segment. If the segment is sinusoidal, the autocorrelation function is a cosine-like function with a minimum at  $\tau/2$  and a maximum at  $\tau$ . The location and extent of such a segment in time are determined by adding or subtracting beginning- and end-date data points from a candidate segment until a cosine pattern appears.

The several subharmonic segments observed in the extended study of *SST3.4* had maxima only during April–May–June (AMJ) or November–December–January (NDJ). When there are time segments in  $aG$  showing a periodicity of a multiple of one year, a complete classification is given by three discrete indices: subharmonic number, parity, and sub-state index [1]. See Appendix B for a review of these defined quantities.

3. **Analysis and discussion**

3.1. *Temperature data from Pacific Region 3.4*

While Region 3.4 is not global, there are two reasons for analyzing it here. Indices derived from it are widely used as a proxy for the study of the El Niño/La Niña phenomenon, and this region is one of the few climate systems where parent data, from which all other properties are derived, is available. In particular, the importance of the annual component will be demonstrated, and characteristics of the seasonally-repaired time series of global data sets will be shown to be virtually the same as those of this region.

It is useful to consider the amplitude of the high-frequency data series  $hG$ , defined as

$$A(hG) = (2 \text{ average}(hG^2))^{1/2}. \tag{6}$$

where the average is over one year, symmetric about the point in question, and  $hG^2$  is the set of squares of the individual numbers in  $hG$ .

Fig. 1 shows the parent data *SST3.4*. Fig. 2a shows the high frequency signal  $hSST3.4$  (thin) and its amplitude  $A(hSST3.4)$  (thick). Fig. 2b contains the autocorrelation of  $hSST3.4$ , which displays a

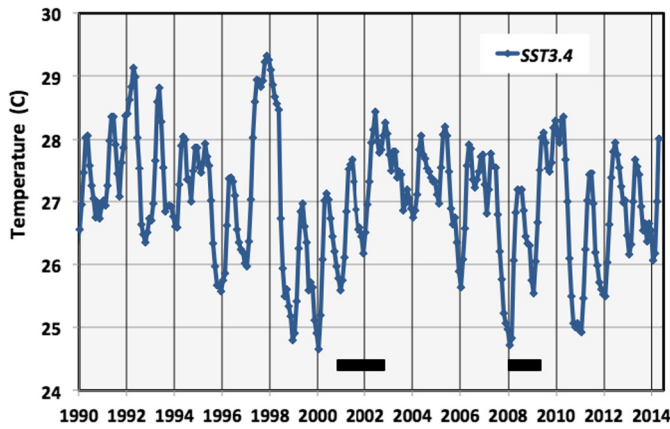


Fig. 1. Parent signal  $SST3.4$ . The climate shifts (CS) during 2001–02 and during 2008–09 from prior studies are indicated by thick black horizontal lines.

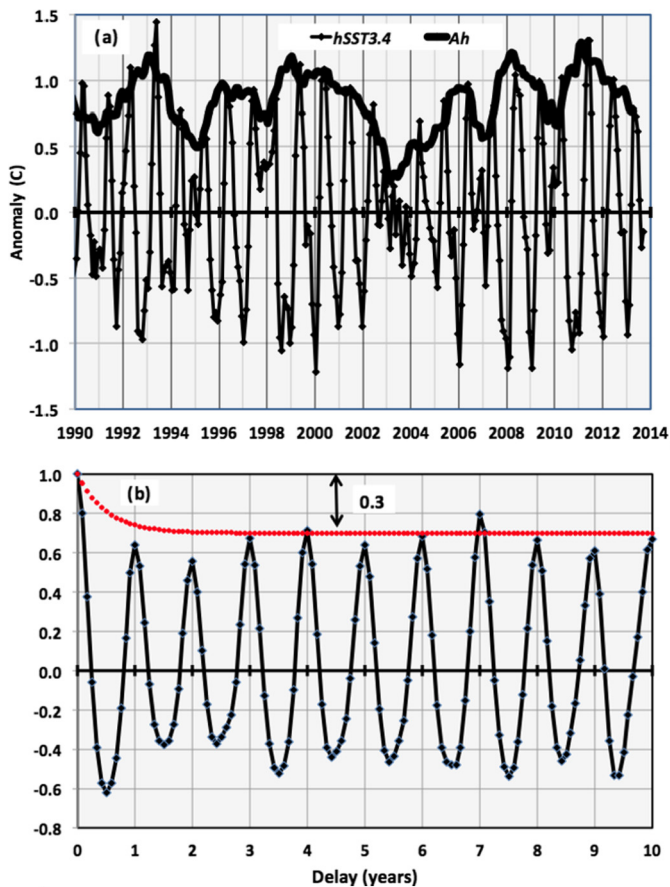
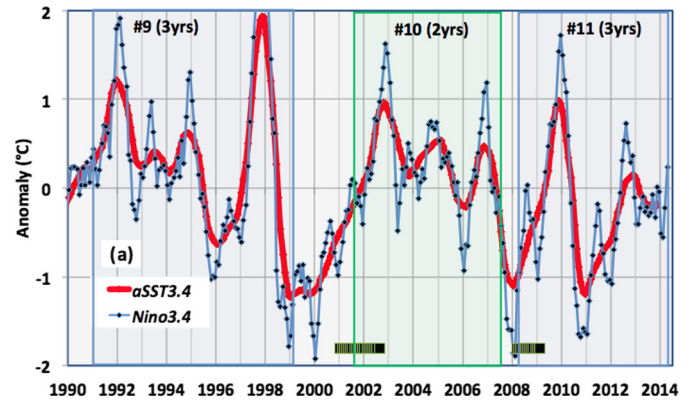


Fig. 2. a. High frequency index  $hSST3.4$  (thin) and its amplitude  $A(hSST3.4)$  (thick). b. Delayed autocorrelation of  $hSST3.4$  showing periodicity of 1.0 cycles/yr and a constant maximum of 0.7 at large delay times.

rapid drop from 1.0 to a sustained oscillation of 1.0 cycle/yr reaching a maximum of  $\sim 0.7$ . The rapid drop is modeled by an exponential decay to the sustained maximum with a characteristic time  $t_e$ . The best fit was for values of  $t_e$  less than 1.0 year. The red curve uses  $t_e = 0.5$  years. The drop of 0.3 from 1.0 is the fraction of the variance of  $hSST3.4$  that one ascribes to stochastic noise.

Fig. 3a shows  $aSST3.4$  and the climatology-generated  $Nino3.4$  index. A search of  $aSST3.4$  for time segments of periodicity that are a multiple of 12 months by the autocorrelation method described in Section 2.4 was performed. Three segments were found: from about 1990 to about 1999 showing 3-year periodicity; from about



1990 1992 1994 1996 1998 2000 2002 2004 2006 2008 2010 2012 2014

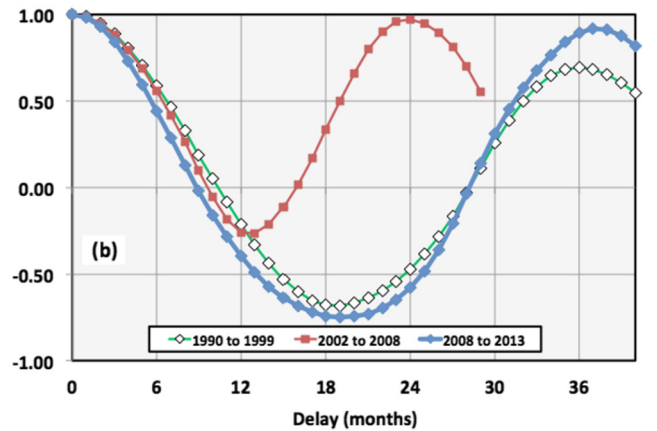


Fig. 3. a. Low frequency index  $aSST3.4$  (red) and NOAA anomaly index  $Nino3.4$  generated by the climatology method (blue). See Section 4 for a discussion. Climate shifts shown as in Fig. 1. b. Autocorrelation of segments of  $aSST3.4$  (see legend for dates), indicating periodicities of 24 months (2002–2008) and 36 months 1990–1999 and 2008–2013). (For interpretation of the references to color in this figure, the reader is referred to the web version of this article.)

2002 to about 2008 showing 2-year periodicity; and a segment from about 2008 to 2013 (end of data) showing 3-year periodicity. The first two segments were reported in [1]; the third is new. All three are indicated by shaded rectangles in Fig. 3a. The numbering of the segments follows [1]. The autocorrelation functions of all three segments, 9, 10, 11, are shown in Fig. 3b. Note that the  $Nino3.4$  index contains several annual peaks, indicating that the climatology method has not been effective in removing them. This will be discussed in Section 4.

The average temperature in each month during a phase-locked segment was computed. For example, during the segment from 1991 to 1999 there were about three oscillations of period 3 years. So each of the 36 months had about three values in the average. This is shown in Fig. 4a (in red), where the maximum in November corresponds to the years 1991, 1994 and 1997 (in black). (Note: the maximum at November 1997 is better known as the El Niño of 1997, the largest such event in a century.) Also shown in Fig. 4a are the 12 averaged values of  $hSST3.4$ . The maximum of  $hSST3.4$  is in May every year.

The same calculations were done for the 2-year segment from 2002 to 2008. The maximum in  $aSST3.4$  occurs during November of 2002, 2004 and 2006. See Fig. 5a. These calculations were also done for the segment from 2008 to 2013 (end), with the results shown in Fig. 6a.

Phase locking is elegantly confirmed by plotting the average monthly values of  $hSST3.4$  versus  $aSST3.4$  during the  $aSST3.4$  phase-locked cycle. One finds closed Lissajous loops where the number of

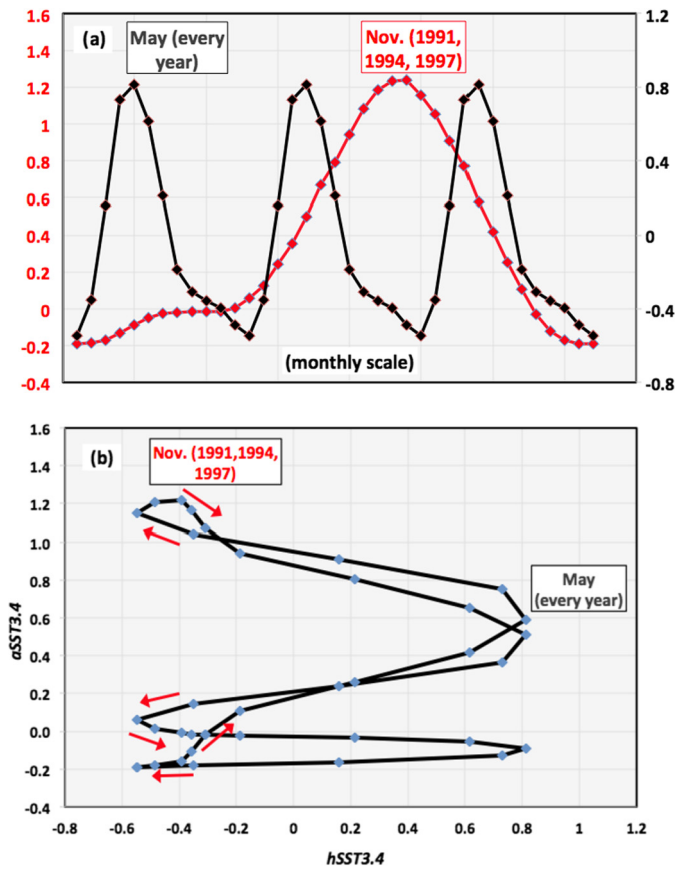


**Fig. 4.** a. Monthly averages of  $aSST3.4$  and  $hSST3.4$  during the 1991–1999 36-month phase-locked state. b. Lissajous plot of the values of  $aSST3.4$  and  $hSST3.4$  from Fig. 4a. (For interpretation of the references to color in this figure, the reader is referred to the web version of this article.)

**Table 1**

Variance ( $^{\circ}C^2$ ), 2000 to 2013. The operations  $a$  and  $h$  are defined in the text. If the annual signal had been successfully removed from  $Nino3.4$ , its variance would be 0.336.

	$G = SST3.4$	$G = Nino3.4$
$G$	0.798	0.574
$hG$	0.336	0.132
$aG$	0.337	0.336

loops is the subharmonic number for that phase-locked segment. See Figs. 4b, 5b, and 6b.

The variances of various quantities associated with  $SST3.4$  are listed in Table 1. These will be discussed below.

3.2. Discussion of results for  $SST3.4$

The data set  $SST3.4$  contains both a high frequency component  $hSST3.4$  and a low frequency component  $aSST3.4$ . Both are necessary to obtain a complete appreciation of the underlying phenomena.

$hSST3.4$ . This index has an amplitude of about  $1^{\circ}C$ . The auto-correlation function shows a sustained oscillation of 1.0 cycle/yr whose amplitude is not decreasing, implying an external forcing  $F_S$ . Since the oscillation frequency is 1.0 cycle/yr,  $F_S$  almost certainly originates in the solar irradiance, which has an annual component of amplitude of  $11.3 W/m^2$ . Its maximum occurs in early January when Earth is at perihelion. The average of the monthly values of  $hSST3.4$  has a maximum during May; one would expect this maximum to occur several months after perihelion, since the temperature of Earth responds to the solar irradiance

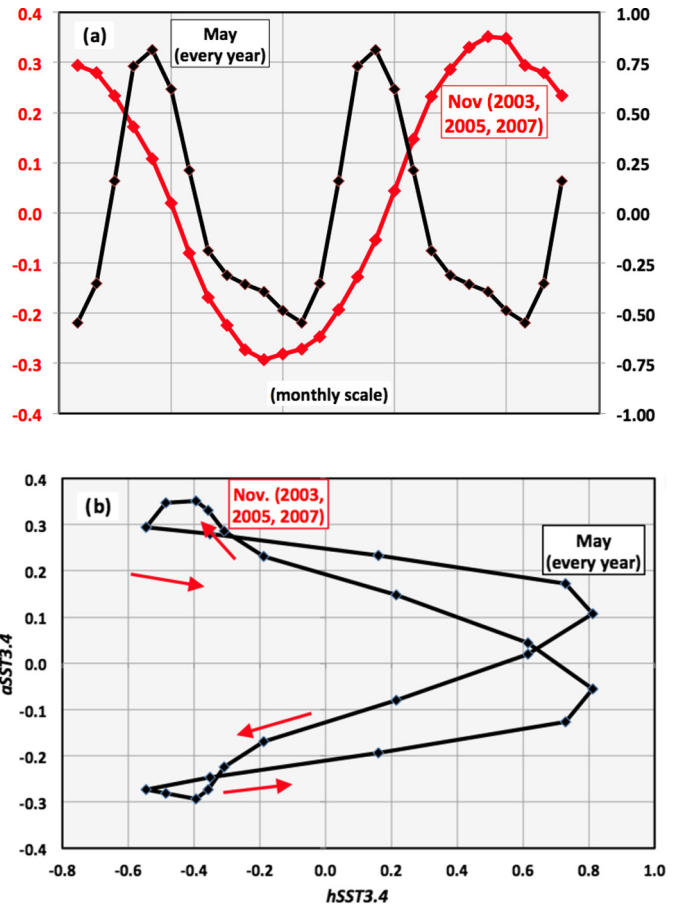


**Fig. 5.** a. Monthly average of  $aSST3.4$  and  $hSST3.4$  during the 2002–2008 24-month phase-locked state. b. Lissajous plot of the values of  $aSST3.4$  and  $hSST3.4$  from Fig. 5a.

with a delay of several months, an effect seen clearly in outgoing longwave radiation (for example, Douglass and Knox [7], Section 5.1).

$aSST3.4$ . This index shows three phase-locked time segments. From 1990 to 1999 it shows phase locking to the annual term at the third subharmonic (period three years). The maxima occur during November during 1991, 1994 and 1997. The classification of this state (Appendix B) is parity *ortho*,  $n = 3$ , and sub-state index  $s = 0$ . Phase locking during this state is decisively demonstrated by the 3-to-1 Lissajous pattern of Fig. 4b. From 2002 to 2008 the index  $aSST3.4$  shows phase locking to the annual term at the second subharmonic (period two years). The maxima occur during November in even numbered years (2002, 2004 and 2006). The classification of this state according to Appendix B is parity *ortho*,  $n = 2$ , and sub-state index  $s = 0$ . Phase locking during this state is dramatically demonstrated by the 2-to-1 Lissajous pattern of Fig. 5b.

It was noted that the time segment of  $aSST3.4$  after 2008 to the end of available data (end of 2013) is consistent with a phase-locked state of period 36 months (3 years,  $n = 3$ ), parity = *ortho*, and sub-state index  $s = 0$  relative to the maximum during segment 9 (1990–1997) [1].

In sum,  $F_S$  causes both  $hSST3.4$  and  $aSST3.4$ .

4. Adverse climatology effect on El Niño/La Niña analyses

Fig. 3a shows the anomaly  $aSST3.4$  used in this study, along with the NOAA index  $Nino3.4$  generated by the climatology method. One sees by inspection that in  $Nino3.4$  there remain fea-

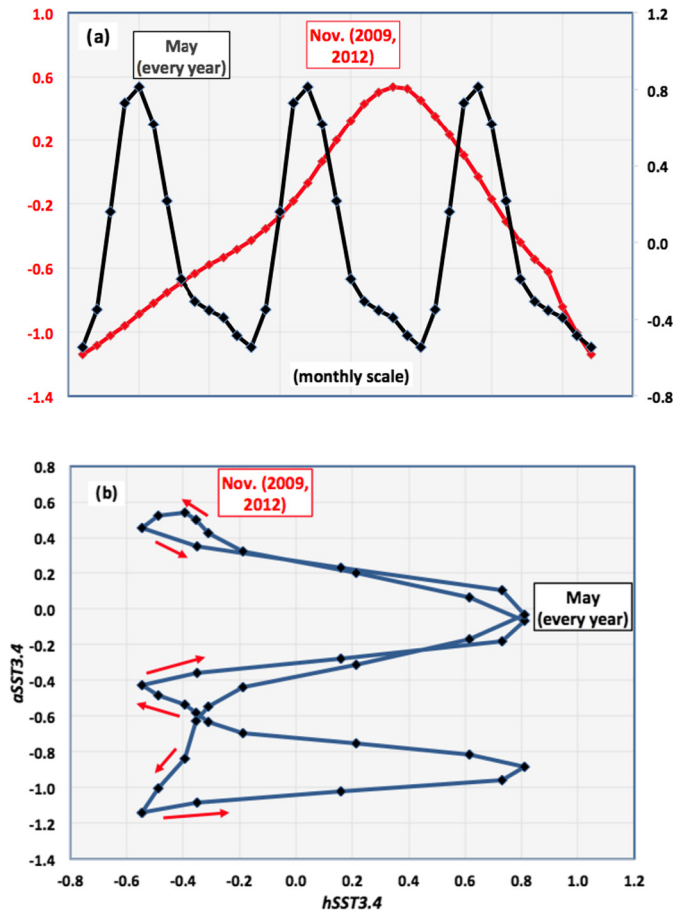


Fig. 6. a. Monthly average of  $aSST3.4$  and  $hSST3.4$  during the 2008–2013 36-month phase-locked state. b. Lissajous plot of the values of  $aSST3.4$  and  $hSST3.4$  from Fig. 6a.

tures that are spaced one year apart. The climatology scheme has not removed the seasonal effect, while the  $F$ -filter has. The climatology scheme can never work because the definition of the climatology function assumes that the amplitude of the seasonal effect is the same for every year. This is not true, as Fig. 2a shows.

For those attempting to understand El Niño/La Niña phenomenon, the climatology-induced features at one-year intervals mask them. For example, in the NOAA report “State of the Climate in 2011” [8], one finds this statement: “... there are multiple definitions that have evolved to describe it. La Niña is described in some sections as a protracted episode ... and in some [other sections] as a ‘double dip’ episode...” This report is explicitly referring to the two minima in  $Nino3.4$  at 2008 and 2009 and the second pair at 2011 and 2012. Clearly, these ‘double dip’ episodes are not present in  $aSST3.4$ . For another example, consider the definition of a warm/cold (El Niño/La Niña) episode, which based upon a threshold of  $\pm 0.5^\circ\text{C}$  in  $Nino3.4$  [9]. Using this definition one finds that there is a warm episode (El Niño) during 2006–07 according to the  $Nino3.4$  index but it is not seen in  $aSST3.4$ . The same conclusions are made for 2013–14. Also, the ‘double dip’ episodes are listed as two distinct cold episodes (La Niñas). These differences can be quantified by comparing the variances of various quantities. From Table 1 one sees that the parent time series  $SST3.4$  has a variance of  $0.798(^\circ\text{C})^2$ . The variances for  $hSST3.4$  and  $aSST3.4$  are  $0.336(^\circ\text{C})^2$  and  $0.377(^\circ\text{C})^2$ , respectively – almost equal in magnitude. The variance of  $Nino3.4$  is  $0.574(^\circ\text{C})^2$ , greater than that for  $aSST3.4$ , showing again that the climatology scheme did not completely remove the seasonal signal. That  $Nino3.4$  contains a high frequency component can be computed in the same way as for

$SST3.4$  – using filter  $F$  to calculate the components,  $hNino3.4$  and  $aNino3.4$ . The variances are  $0.132(^\circ\text{C})^2$  and  $0.336(^\circ\text{C})^2$  respectively. Thus, in terms of the variance, about 23% of  $Nino3.4$  comes from the presence of the unwanted seasonal effect. As expected from Eq. (5), calculation of the time series  $F(Nino3.4)$  shows it to be exactly the same as  $aSST3.4$ .

### 5. Origin of the observed phase locking

In his report of ten sequentially-numbered phase-locked states of periods two and three years, Douglass [1] pointed out that the phenomenon of subharmonic phase locking is well known in the field of nonlinear dynamics. It indicates the presence of a nonlinear interaction within the system. He referred to Stoker [10], who illustrated this by considering the forced one-dimensional oscillator with empirically added nonlinear terms in the restoring force. These terms are responsible for the subharmonics.

Several attempts toward a realistic first-principles theory of ENSO have been published. In 1985 Cane and Zebiak [11] (CZ) proposed a coupled tropical ocean–atmosphere model of El Niño and Southern Oscillation that has been used by later investigators. In 1994–95 three papers based upon CZ were published nearly simultaneously [12–14]. These later models had both an external forcing at 1.0 cycles/yr and nonlinear coupling terms. The nonlinearities considered involved such variables as westerly winds and poleward transport of heat. They all predicted some form of chaotic behavior, which was manifested in the appearance of stable subharmonics for certain values of adjustable parameters. The nonlinearities in these models are all different and none vary the nonlinear terms that correspond to the observations. Chang et al. [14], in fact, found that when they varied the amplitude of the “heat flux” parameter in their model, subharmonics at two- and three-year periods appeared within certain amplitude ranges.

### 6. Conclusions and summary

Phase-locked sequences are found in Pacific Ocean  $SST3.4$  temperature data during the periods 1991–1999, 2002–2008 and in 2009–2013. These three sequences apparently being separated by climate shifts. It is asserted that the associated climate system is driven by a forcing of solar origin that has two manifestations: (1) A direct phase-locked response to what is identified as a solar forcing at a frequency of 1.0 cycle/yr for the whole time series; (2) A phase-locked response at either the second or third subharmonic of the putative solar forcing between 1991 and 1999; 2001–02 and 2008; and again between 2008 and 2013.

This study confirms the results of [1] that some of the largest maxima/minima in the oscillations of the phase-locked state correspond to well-known El Niños/La Niñas. For example, the sequence 1996 La Niña – 1997/98 El Niño – 1999 La Niña corresponds to a minimum–maximum–minimum portion of phase-locked segment #9. The climate system is presently (June 2014) in a phase-locked state of periodicity 3 years. This state, which began in 2008, contains a maximum (El Niño) at about 2010 followed by a minimum (La Niña) followed by a maximum (weak El Niño at about 2013). If the climate system remains in this phase-locked state, the next maximum will not occur until about 2016 – i.e., no El Niño before that date. On the other hand, if a maximum occurs before then, it will signal the end of the phase-locked segment (and therefore a climate shift).

On its web site [15] the National Oceanic and Atmospheric Administration asks: “How often does La Niña occur?” Answer: “El Niño and La Niña occur on average every 3 to 5 years. However, the historical record the interval between events has varied from 2 to 7 years. ...” Our findings show that during phase-locked time segments the pe-

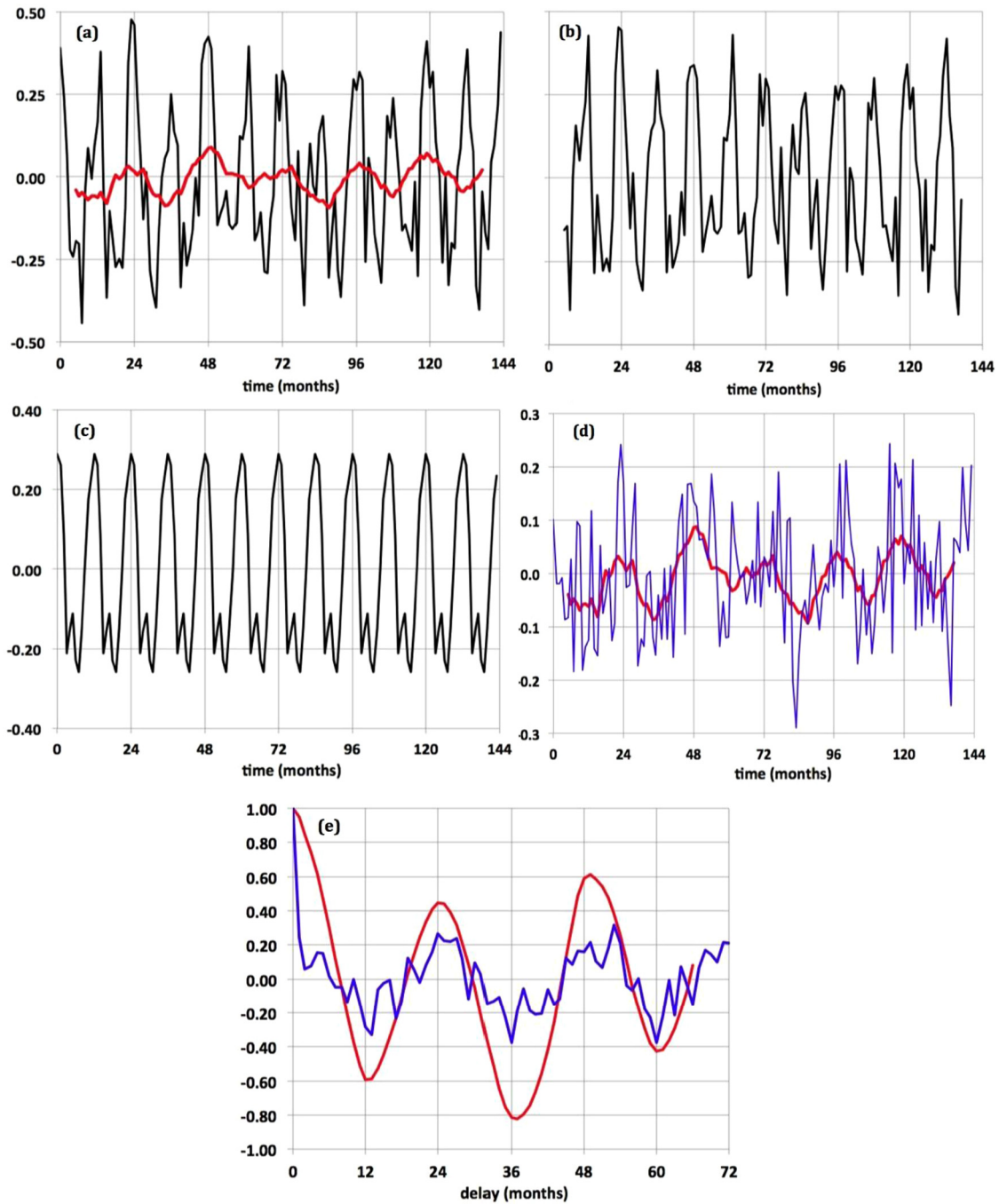


**Fig. A.1.** a. A sample series  $G$  (Eq. (A.1), black) and the hidden component (Eq. (A.4), red) as approximated by 12-month filtering that produces  $F(G) = aG$ . b. The high-frequency component  $hG$ , which is the difference between the black and red curves of Fig. A.1a. c. The climatology function  $C(G)$ , Eq. (A.7). d. A comparison of the relative success of the 12-month filter  $F$  (red) with that of the climatology method (blue). e. Autocorrelation functions of  $aG$  (red) and  $aG_C$  (blue), showing their 24-month period. (For interpretation of the references to color in this figure, the reader is referred to the web version of this article.)

riod is either 2 or 3 years. If a longer interval is observed, this is not representative of a variable ‘period,’ but indicates the occurrence of a climate shift between phase-locked segments.

It is pointed out that the 12-month moving average filter is demonstrably superior to the climatology method of removing seasonal effects in data. This is seen to be the case for interpretation of El Niño/La Niña data, which contains spurious annual effects when treated under the climatology scheme.

An extension of these results to global data will be presented in a second Letter [16]. It will be shown that patterns of sub-harmonics identical to those described here occur throughout the oceans.

**Appendix A. Illustration of filtering procedures**

To demonstrate the comparative action of the climatology and 12-month moving filters, we constructed a noisy time series  $G(t)$  consisting of an annual signal  $A(t)$ , a biannual “signal of interest”  $B(t)$  and a random sequence  $R(t)$  on the interval  $t = 1$  to 144 in the form of a monthly series of 144 points:

$$G(t) = A(t) + B(t) + R(t), \tag{A.1}$$

where, with  $t$  represented by  $k$  in months,

$$A(t) = 0.2 \sin(2\pi k/12) + 0.4 \sin(4\pi k/12), \tag{A.2}$$

$$B(t) = 0.1 \sin(\pi(k+3)/12), \quad (\text{A.3})$$

and

$$R(t) = 0.4 \text{rand}(k), \quad (\text{A.4})$$

where  $\text{rand}(k)$  is a set of random numbers in the range  $-0.5$  to  $+0.5$ . This set and implementations of this demonstration were obtained with MATLAB<sup>®</sup>.

Fig. A.1a shows the series  $G$  and the filtered series  $F(G) = aG$ . The zero values in  $aG$  at each end represent missing numbers due to the nature of the 12-month filter. The “signal of interest”  $B(t)$ , the red curve, has been successfully separated from the annual signal although suffering the appearance of some noise. The noise also appears in the autocorrelation (Fig. A.1e) in a different form, namely, a damping of the amplitude of the curve.

A climatology function  $C(G)$  is constructed as follows (see Section 2.1): a “month  $j$ ” average is formed:

$$c(j) = \frac{1}{12} [G(j) + G(j+12) + \dots + G(j+132)], \quad (\text{A.5})$$

and a series is built from these,

$$m(G) = [c(1)c(2) \dots c(12)], \quad (\text{A.6})$$

followed by

$$C(G) = [m(G)m(G) \dots (\text{total of 12 terms}) \dots m(G)], \quad (\text{A.7})$$

a set of obvious one-year periodicity. The climatology correction to  $G$  is then constructed as  $aG_C = G - C(G)$ .

Fig. A.1a shows the sets  $G$  and  $aG$ . The “hidden signal”  $B(t)$  (in red) is reproduced with a smaller amplitude and a few distortions induced by the noise. Fig. A.1b shows the high-frequency component  $hG = G - aG$ . Fig. A.1c is a plot of the climatology function  $C(G)$  (Eq. (A.7)), and Fig. A.1d compares sets  $aG$  (in red) and  $aG_C$  (in blue). While there is evidence of the hidden signal in  $aG_C$ , the poorly removed noise prevents a good characterization of it. The 2-year periodicities are better illustrated in Fig. A.1e, which shows autocorrelations of  $aG$  (in red) and  $aG_C$  (in blue).

The red curve of Fig. 3a illustrates the application of this filtering technique to observational data.

## Appendix B. Formal notation for phase-locked segments [1]

*Subharmonic number  $n$ .*  $n$  is the period, in years, of one oscillation of  $aG$ .

*Parity.* A parity *ortho* is assigned if maxima occur during NDJ and *para* if they occur during AMJ.

*Sub-state index  $s$ .* Consider two similar segments having the same subharmonic number and parity, separated by  $Y$  years as measured between the first maxima of the segments. Since  $Y$  is not necessarily a multiple of  $n$ , a third descriptor  $s$  is defined by  $s = Y \pmod{n}$ , whose values are  $0, 1, \dots, n-1$ . Thus a segment with period 3 years has three possible equivalent “sub-states” indexed by 0, 1, and 2. For an example with  $n = 3$ , see Section 4.2 of Ref. [1]. Since the sub-state index depends on the choice of a reference year, for which it is defined as 0, it is relative, used only in comparing segments of the same  $n$  and parity.

## References

- [1] D.H. Douglass, Phys. Lett. A 376 (2011) 128–135, <http://dx.doi.org/10.1016/j.physleta.2011.10.042>.
- [2] D.H. Douglass, Phys. Lett. A 374 (2010) 4164–4168, <http://dx.doi.org/10.1016/j.physleta.2010.08.025>.
- [3] D.H. Douglass, Phys. Lett. A 377 (2013) 1749–1755, <http://dx.doi.org/10.1016/j.physleta.2013.04.053>.
- [4] NOAA/CPC, SST3.4 data and indices are found at <http://www.cpc.ncep.noaa.gov/data/indices/>, 2013.
- [5] D.H. Douglass, Int. J. Geosci. 2 (2011) 414–419, <http://dx.doi.org/10.4236/ijg.2011.24045>.
- [6] S.W. Smith, The Scientists and Engineer's Guide to Signal Processing, California Technical Publishing, San Diego, 1997.
- [7] D.H. Douglass, R.S. Knox, Phys. Lett. A 373 (2009) 3296–3300, <http://dx.doi.org/10.1016/j.physleta.2009.07.023>.
- [8] NOAA, State of the climate in 2011. Go to <http://www.ncdc.noaa.gov/bams-state-of-the-climate/2011.php>, 2012.
- [9] NOAA/CPC, Cold and warm episodes at [http://www.cpc.ncep.noaa.gov/products/analysis\\_monitoring/ensostuff/ensoyears.shtml](http://www.cpc.ncep.noaa.gov/products/analysis_monitoring/ensostuff/ensoyears.shtml), 2013.
- [10] J.J. Stoker, Nonlinear Vibrations, Interscience Publishers, 1950.
- [11] M.A. Cane, S.E. Zebiak, Science 228 (1985) 1085–1087.
- [12] F.-F. Jin, J.D. Neelin, M. Ghil, Science 264 (1994) 70–72.
- [13] E. Tziperman, L. Stone, M.A. Cane, H. Jarosh, Science 264 (1994) 72–74.
- [14] P. Chang, L. Ji, B. Wang, T. Li, J. Atmos. Sci. 52 (1995) 2353–2372.
- [15] NOAA. Go to [http://noaa.gov/lanina\\_new\\_faq.html](http://noaa.gov/lanina_new_faq.html), 2014.
- [16] D.H. Douglass, R.S. Knox, Phys. Lett. A (2015), <http://dx.doi.org/10.1016/j.physleta.2014.10.058>, in press.

Note: All papers authored by Douglass/Knox may be found at <http://www.pas.rochester.edu/~douglass/recent-publications.html>.